Optical Characterization of a Ferroelectric Liquid Crystalline Polymer Studied by Time-Resolved Optical Waveguide Spectroscopy

Masaya Mitsuishi, Shinzaburo Ito, and Masahide Yamamoto*

Department of Polymer Chemistry, Graduate School of Engineering, Kyoto University, Sakyo, Kyoto 606-8501, Japan

Hiroyuki Endo and Satoshi Hachiya

Central Research Laboratories, Idemitsu Kosan Co., Ltd., 1280 Kamiizumi, Sodegaura, Chiba 299-02, Japan

Thomas Fischer

Fakultät für Physik, Universität Leipzig, Linnéstrasse 5, D-04103 Leipzig, Germany

Wolfgang Knoll

Max-Planck-Institut für Polymerforschung, Ackermannweg 10, D-55128 Mainz, Germany, and The Institute of Physical and Chemical Research (RIKEN), Frontier Research Program, 2-1 Hirosawa, Wako, Saitama 351-01, Japan

Received September 29, 1997; Revised Manuscript Received January 5, 1998

ABSTRACT: The static structures and switching dynamics of a side chain ferroelectric liquid crystalline polymer (PSiOFLC) were investigated by using time-resolved optical waveguide spectroscopy (TROWS). A good alignment of the mesogenic side chains was obtained by a shearing procedure. The liquid crystalline phases of PSiOFLC were characterized by determining the dielectric tensor diagonals of PSiOFLC, in which the contribution of the main chain to the optical anisotropy could be neglected. The PSiOFLC layer in the S_A phase could be treated as a uniaxial refractive index ellipsoid which aligned parallel to the substrate plane with bookshelf structure. The PSiOFLC layer in the S_{C^*} phase under the large electric field was also considered as a uniaxial ellipsoid model. The transient waveguide mode patterns of PSiOFLC were successfully obtained with a millisecond time resolution. During the reorientation, the smectic layer structure changed from bookshelf to chevron and then back to the bookshelf structure. The slowness of the switching time was attributed to a "polymer effect" in which the polymer backbones lying in the smectic layer plane act as a "hook" to restrict the motion of side chains due to the binding of the mesogenic moieties to the polymer backbone, resulting in the increase of viscosity.

Introduction

Ferroelectric liquid crystalline polymers (FLCP) have attracted much attention, e.g., in nonlinear optics, optical storage, electrooptic devices, and large area liquid crystal (LC) displays. Side chain FLCPs have been extensively synthesized and studied by various groups for 1 decade.[1−15] The backbones of these polymers are flexible chains such as polyacrylates,[1−3,6,15] polymethacrylates,[1−3,6,8,11,12] polysiloxanes,[7,9−12] poly(vinyl ethers),[13] and poly(oxyethylenes).[14] The mesogenic moieties which show ferroelectricity in the low molecular mass LC are attached to the polymer backbone through a flexible spacer. The static behavior in the FLCP has been studied not only in the bulk but also in the monolayer, using optical microscopy, X-ray diffraction, and differential scanning calorimetry.[16−25]

As for the study of the dynamic properties of these polymers, time-resolved Fourier transformed infrared (FT-IR) spectroscopy[26−28] has revealed that the polymer backbone moves with the motion of the mesogenic side chains under an external electric field. Here we describe the optical characteristics of a side chain FLCP in each phase. The dynamics of the polymer under an alternating electric field have been investigated through the analysis of the transient data of time-resolved optical waveguide spectroscopy (TROWS).

Experimental Section

Sample Preparation. The molecular structure of the sample used is given below. The polymer has a polymethylsiloxane main chain containing alkyl spacer and (2*S*)-2-methylbutyl 4-(4′-hydroxybenzoyloxy)benzoate mesogenic side groups. The molecular weight was about 30 000, which was obtained by gel permeation chromatography (GPC) and calculated using a polystyrene standard; one polymer chain consists of ca. 50 monomer units. Hereafter the polymer is abbreviated as PSiOFLC. The phase transition temperatures of PSiOFLC were determined by polarized microscopy as summarized below the chemical structure. The range of the S_{C^*} phase is much wider than that of the relevant low molecular mass ferroelectric liquid crystal (FLC) due to the polymerization of monomeric mesogen groups.

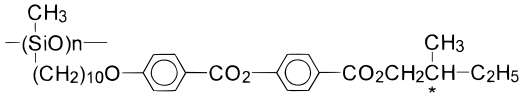

$Mw = 3.2 \times 10^4$, $Mn = 2.5 \times 10^4$, $Mw/Mn = 1.28$

Iso - 132°C - SmA - 107°C - SmC*

PSiOFLC

* To whom correspondence should be addressed. E-mail: a50471@sakura.kudpc.kyoto-u.ac.jp.

S0024-9297(97)01433-2 CCC: $15.00
Published on Web 02/13/1998

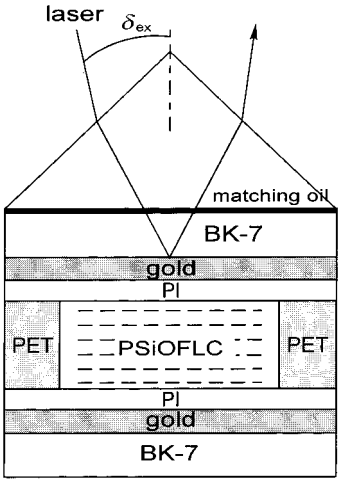

Figure 1. Schematic illustration of the sample cell structure used in the current study. The polyimide (PI) layer was not rubbed. The thickness of each layer is listed in Table 1.

An optical waveguide cell of PSiOFLC was fabricated as explained previously.[29] The PSiOFLC was sandwiched between two glass plates by a capillary effect at the isotropic phase above 140 °C; it took 7−8 h for preparation. A polyester (PET) film was used as a spacer. The cell spacing was adjusted to keep the number of the interference fringes observed on the top gold layer as small as possible.

For investigating the molecular reorientation of the FLCP, it is vital but often difficult to obtain a well-aligned optical cell. In the present case, rubbing of the precoated alignment layer was not useful. We tried to orient the mesogenic groups by applying an alternating shearing force[30] along one direction at the isotropic−S_A phase transition temperature during the cooling process at 0.2 °C/min, but severe damage of the gold layers and distortion of the uniform cell spacing often occurred. The polyimide (PI, AL1524H, Japan Synthetic Rubber Co.) layer was coated to a thickness of ca. 150 nm, and the thickness of PSiOFLC was approximately 7.0 μm so as not to damage the optical cell. The cell thus obtained was coupled with a right-angle prism (BK-7) by using index matching oil as illustrated in Figure 1.

Measurement. The procedure of the optical waveguide measurement to obtain an angle-dependent reflectivity (not time-resolved) has been outlined previously.[31] In this section, only the time-resolved measurement for the PSiOFLC cell is explained.

The time-resolved measurement was performed in the S_{C^*} phase. As an incident beam, linearly polarized light from a He−Ne laser (632.8 nm) impinged on the PSiOFLC cell. An alternating rectangular voltage was applied to the PSiOFLC cell from a function generator. The signal, i.e., the intensity of the reflected light from the prism coupler was detected by a photodiode and time-resolved through a transient memory synchronized with the applied voltage. We did not use a polarizer in front of the photodiode; thus, the total reflectivity, not a component of polarization, was monitored in the measurement. The increment of the incident angle was fixed at 0.2°, and acquisition of the signal was repeated seven times with a 3.0 ms time resolution; 1.5 h was needed for scanning the incident angle from 35° to 55°. As for polarization of the incident beam, either a TE (transverse electric) field or TM (transverse magnetic) field, i.e., *s*- or *p*-polarization was used.

Coordinate System. The coordinate system of the sample cell with respect to the laboratory measurement coordinate system is as follows. The polarized microscopic observation revealed that in the S_A phase the mesogenic side chains were aligned toward the direction perpendicular to the shear direction. Therefore as shown in Figure 2(a), the *Y* axis is set to coincide with the shear direction. The direction of the incident light beam is given by the angle β between the *X* axis and the projection of the light beam on the *XY* plane. This means that at $\beta = 0°$ the plane of incidence is parallel to the smectic layer normal (parallel to the director of mesogenic group), while at $\beta = 90°$ the plane is perpendicular to the director.

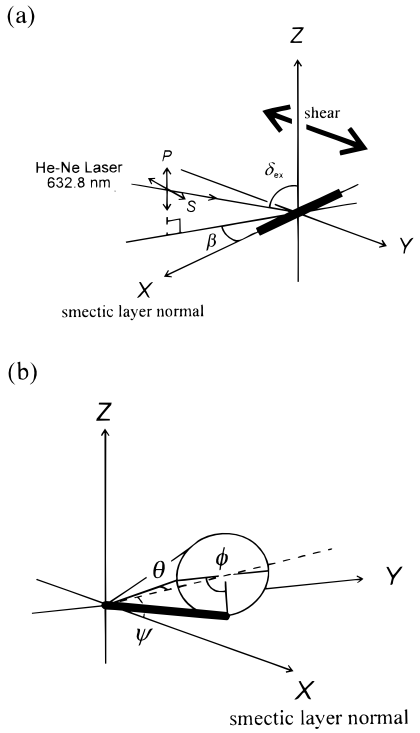

Figure 2. (a) Coordinate system for the optical waveguide measurement. The black rod depicts the director in the S_A phase; (b) The coordinates of the director of PSiOFLC in the S_{C^*} phase. Three angles (θ, ϕ, ψ) represent the cone angle, the azimuthal angle, and the smectic layer tilt angle.

Table 1. Optical Parameters for Each Layer in the Isotropic Phase at $T = 139$ °C

	BK-7	Au(top)	Au(bottom)	PI	PSiOFLC
ϵ' [a]	2.296	−11.818	−11.816	2.560	2.289
ϵ'' [b]	0.000	1.433	1.254	0.000	0.000
d [c] (nm)		31.8	44.2	143.7	7479

[a] The real part of the optic dielectric constant. [b] The imaginary part of the optic dielectric constant. [c] The thickness of each layer.

Results and Discussion

1. Optical Characterization of Each Phase. 1.1. Isotropic Phase. Figure 3 parts a and b show waveguide mode patterns in the isotropic phase at $T =$ 139 °C. The polarization of the incident light was, respectively, (a) *s*-polarization or (b) *p*-polarization. Since PSiOFLC is optically isotropic at $T = 139$ °C, the polarization of the incident light was kept in the reflected light, which resulted in a series of sharp dips in parts a and b of Figure 3. The optical parameters of each layer except for the PSiOFLC layer were determined by the surface plasmon and the optical guided wave measurement before inserting the PSiOFLC between the two substrates. The refractive index of PSiOFLC at $T = 139$ °C was evaluated from the fitting with the curve calculated by the Fresnel theory[32] (solid lines in parts a and b of Figure 3). The thickness of the PSiOFLC was precisely determined as 7.479 μm. All these parameters are summarized in Table 1.

1.2. S_A Phase. In the S_A phase the mesogenic groups form the so-called bookshelf structure in which they tend to align toward the direction perpendicular to the

shearing direction and parallel to the substrate plane as mentioned in the Experimental Section. In a polymer system, as observed by neutron scattering and X-ray diffraction measurements,[33] the main chains are normally located between the mesogenic layers, orienting perpendicular to the direction of mesogenic long axis. These facts indicate that both the optical anisotropies of the main chains and side chains must be taken into account in the S_A phase. However, it is still ambiguous how the polymer backbones as well as the mesogenic side chains affect the optical anisotropy in the S_A phase. The contribution of the polymer backbone to the optical anisotropy remains to be estimated.

To evaluate the optical anisotropy of the polymer backbone, the intrinsic (or specific) birefringence of the chemical bonds is evaluated with

$$\Delta n_0 = n_c - n_a = \frac{2\pi N\rho}{9M}(n^2+2)^2(\alpha_c - \alpha_a)/n \quad (1)$$

where Δn_0 is intrinsic birefringence, n_c and n_a are refractive indices parallel and perpendicular to the bond direction, respectively, N is Avogadro's number, ρ is density; M is molecular weight per bond unit, n is refractive index of the material, and α_c and α_a are molecular polarizabilities parallel and perpendicular to the bond direction. It should be noted that n_c and n_a are the values when the polymer backbone is perfectly stretched out while n is the averaged value. The following values were used in order to obtain the intrinsic birefringence for the backbone of Si−O bonding: $M = 74.1$ for the monomer unit, $\rho = 0.970$, $n = 1.4035$ and $\alpha_c - \alpha_a = 0.96 \times 10^{-25}$ cm^3 from the published data for poly(dimethylsiloxane),[34] resulting in the value $\Delta n_0 = 0.0061$. The physical meaning of the intrinsic birefringence Δn_0 is that it is the maximum value when the main chains perfectly align along one direction (presumably shearing direction in this case). The magnitude of Δn_0 obtained seems rather small compared with those for other polymer backbones (e.g., 0.21 for polyester, 0.060 for nylon, 0.058 for polyethylene, and so on). This implies that the siloxane chain has very little birefringence effect on the optical anisotropy of PSiOFLC in the S_A phase; that is, the polymer backbone acts as an isotropic medium in the S_A phase from the optical point of view. This conclusion allows us to employ the model that the refractive indices of PSiOFLC can be regarded as a refractive index ellipsoid, the anisotropy of which is mostly attributed to the orientation of the mesogenic side chain groups. Herein the optic tensor of PSiOFLC in the liquid crystal phase is defined as diagonal components ϵ_{xx} parallel to the mesogenic long axis and ϵ_{yy} and ϵ_{zz}, perpendicular to it.

Figure 4 shows waveguide mode patterns for (a) *s*-light and (b) *p*-light in the S_A phase at $T = 120$ °C and $\beta = 90°$ at which the probe beam propagates perpendicular to the direction of the mesogenic units. Waveguide mode patterns were obtained from two directions of incident light at $\beta = 0°$ and 90° (the result of $\beta = 0°$ was not shown here) using *s*- and *p*-light. At $\beta = 90°$ the incident light polarization coincides with the principal axes of the optic dielectric diagonals of PSiOFLC. Therefore, there was no optical coupling between *s*- and *p*-polarized fields, giving rise to a simple waveguide mode pattern similar to that in Figure 3; no additional shallow dips appeared. For the radiation of *s*-light from $\beta = 90°$, only one component of the optic dielectric tensor of the PSiOFLC, ϵ_{xx}, contributes to the

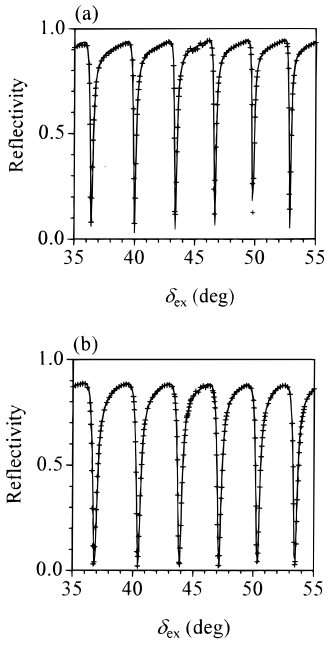

Figure 3. Waveguide mode patterns in the isotropic phase at $T = 139$ °C for (a) *s*-light and (b) *p*-light.

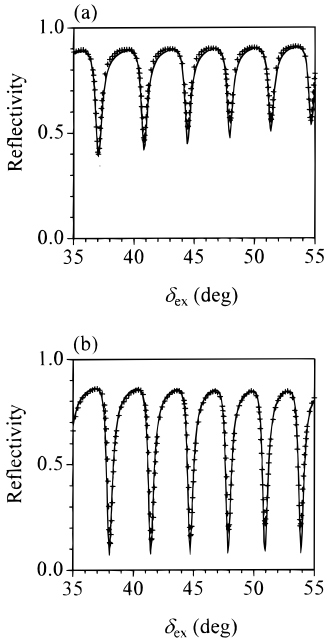

Figure 4. Waveguide mode patterns in the S_A phase at $T = 120$ °C for (a) *s*-light and (b) *p*-light.

Table 2. Optic Dielectric Diagonals of PSiOFLC in the S_A Phase at $T = 120$ °C

	ϵ_{xx}	ϵ_{yy}	ϵ_{zz}
ϵ'	2.542	2.257	2.257
ϵ''	0.005	0.002	0.002

waveguide mode pattern shown in Figure 4a, whereas for *p*-light ϵ_{yy} and ϵ_{zz} relate to the waveguide mode pattern in Figure 4b. The solid curves shown in parts a and b of Figure 4 were calculated with the Fresnel equation[32] and the obtained dielectric diagonals (ϵ_{xx}, ϵ_{yy}, ϵ_{zz}) were summarized in Table 2. The theoretical curves in both parts a and b of Figure 4 are in good agreement with the experimental data. From these results, the PSiOFLC in the S_A phase can be expressed by a uniaxial optical ellipsoid model where the mesogen long axis is

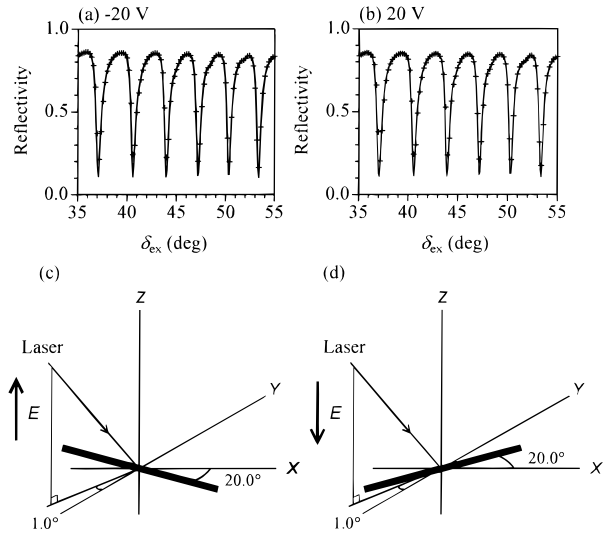

Figure 5. Top: Waveguide mode patterns for *p*-light in the S_{C^*} phase at $T = 95$ °C under an electric field of (a) −20 V and (b) +20 V. Bottom: geometry used for the calculation of the solid lines in the upper parts of Figure 5.

oriented toward the direction parallel to the substrate. The waveguide mode pattern was broader than that in the isotropic phase, in particular for *s*-light. This could be caused by the inhomogeneity of molecular orientation and cell spacing resulting from the shearing procedure. In this instance, we introduced a small amount of imaginary part into the optic dielectric diagonals in order to reproduce the experimental data. These are also listed in Table 2, but it should be mentioned that these imaginary values are apparent and would be zero if the alignment technique is more improved. There are some differences in the imaginary part between the parallel and perpendicular components. This will be discussed later.

1.3. S_{C^*} Phase. In the S_{C^*} phase are tilted the mesogenic moieties from the smectic layer normal, and the tilted director is turned with a given constant azimuthal angle in passing from one layer to the next. Consequently the trace of the director forms a helix. The layer structure is also deformed from a bookshelf to a so-called chevron geometry where the smectic layer is bent at the middle of two substrates. When a large external electric field is applied to the PSiOFLC cell, the helicoidal structure of the director is unwound and the layer structure can be rearranged from the chevron to the bookshelf structure as well as in the case of the low molecular mass FLC (3M2CPOOB),[29] making the analysis in the S_{C^*} phase easier. In practice, a sufficient large electric voltage ±20 V was applied to the PSiOFLC cell. An attempt to apply a voltage larger than 20 V was unsuccessful because such a high electric field gave rise to destruction of the smectic layer, probably due to ionic impurities. The contribution of the polymer backbone to the optical anisotropy was also assumed to be negligible in the S_{C^*} phase.

Figure 5 shows waveguide mode patterns for *p*-light under an electric field of (a) −20 V and (b) +20 V. These patterns were obtained at $\beta = 90°$ and $T = 95$ °C. Because the director of PSiOFLC is titled away from the *X* axis, the effect of off-diagonal components of the dielectric ellipsoid must appear in the waveguide mode patterns, which would cause additional dips due to the *p*−*s* coupling in the PSiOFLC layer. In the present case, however, no additional dips were observed in both

Table 3. Optic Dielectric Diagonals of PSiOFLC in the S_{C^*} Phase at $T = 95$ °C[a]

	ϵ_{xx}	ϵ_{yy}	ϵ_{zz}	θ (deg)
−20 V	$2.605 + 0.006i$	$2.263 + 0.002i$	$2.263 + 0.002i$	20.0
+20 V	$2.605 + 0.006i$	$2.263 + 0.002i$	$2.263 + 0.002i$	20.0

[a] The angle θ is the cone angle. The PSiOFLC layer has a thickness of 7.565 μm. This means that the amplitude of the electric field was 2.64×10^4 V/cm.

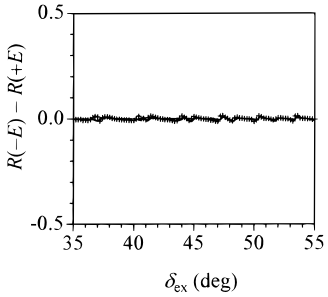

Figure 6. Subtraction of the waveguide mode patterns $R(-E) - R(+E)$ for *p*-light.

parts a and b of Figure 5. This is due to the optical parameters of the PSiOFLC layer, i.e., the thickness and the refractive indices given in Table 3, which made the *p*−*s* coupling very weak. The solid curves were calculated with the geometry depicted in the lower sections of parts a and b of Figure 5 using the optical parameters summarized in Table 3.

The experimental data in parts a and b of Figure 5 suggest that the waveguide mode patterns are identical since the orientation of directors at $E = \pm 20$ V is symmetric with respect to the plane of incidence as shown in parts c and d of Figure 5, but the detailed analysis clearly shows that there are slight differences between two waveguide mode patterns for the alternating electric field. Figure 6 shows the plots of $R(-E) - R(+E)$ for *p*-light where $E = \pm 20$ V. Although we set angle β to be exactly 90°, the real direction of the incident light was 1.0° away from the *Y* axis, as denoted in parts c and d of Figure 5, which is the experimental limit for the accuracy of setting angles. The theoretical curves are in good agreement with the experimental data in Figures 5 and 6.

The director was tilted by 20.0° away from the smectic layer normal (the *X* axis) with the bookshelf geometry. The thickness of the PSiOFLC was also evaluated as 7.565 μm, that is, the amplitude of the applied electric field was 2.64×10^4 V/cm. The results imply that under the high electric field the optic dielectric diagonals of PSiOFLC can be treated as a uniaxial ellipsoid model aligned parallel to the substrate.

2. Switching Process. Our goal is to understand the molecular motion of the PSiOFLC under the influence of the alternating electric field. For example, (1) how does the mesogenic side chain hanging on the polymer backbone rotate around the cone? (2) What kind of conformation can be considered from the molecular motion of the PSiOFLC? Figure 7a shows time-resolved waveguide mode patterns for *s*-light. The cell alignment was the same as that in Figure 5: $\beta = 90°$. An alternating large electric field $V_{pp} = 5.29 \times 10^4$ V/cm and 1 Hz frequency was applied to the PSiOFLC cell. The values given on the right side of each graph indicate the time after the reversal of the polarity of the electric field from -2.64×10^4 to $+2.64 \times 10^4$ V/cm. The time response of the PSiOFLC was seen in several tens of

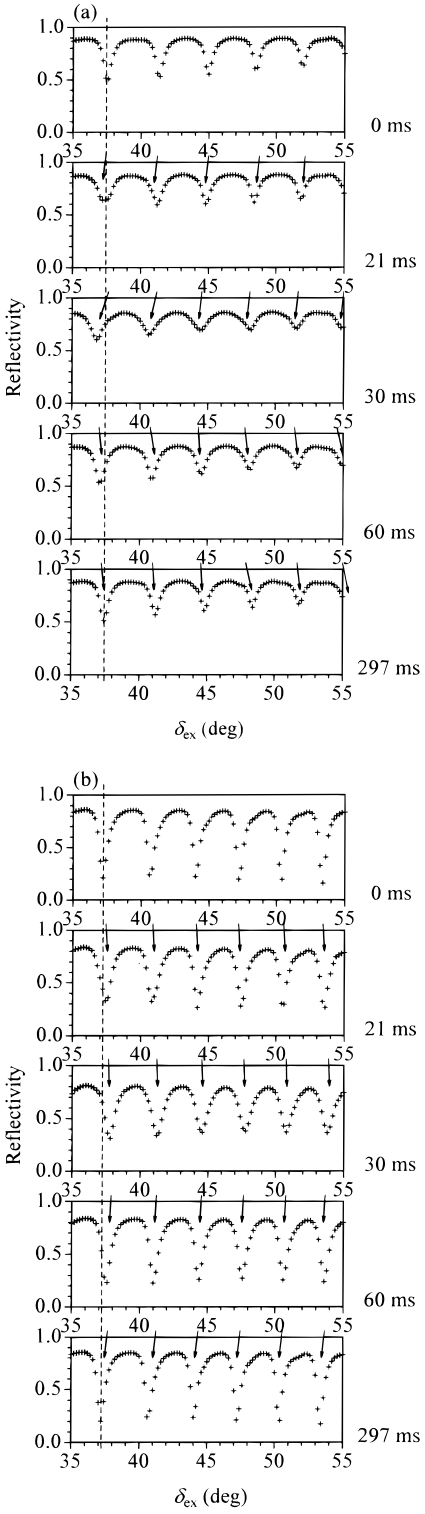

Figure 7. Time-resolved waveguide mode patterns for (a) *s*-light and (b) *p*-light. The geometry of the incident light was the same as that in Figures 5: $\beta = 90°$.

millisecond range. The reason for the slowness will be discussed in section 2.5. Judging from the position of the resonance angle in Figure 7a, the resonance angles shift toward smaller angles until 30 ms and then return to the original positions in around 300 ms. The angle shift is only 1.0° at maximum and the waveguide mode patterns seem to change monotonically. However, this slight change does include detailed information about the switching dynamics of the PSiOFLC mesogenic side chains. As shown in Figure 7b, we measured the other

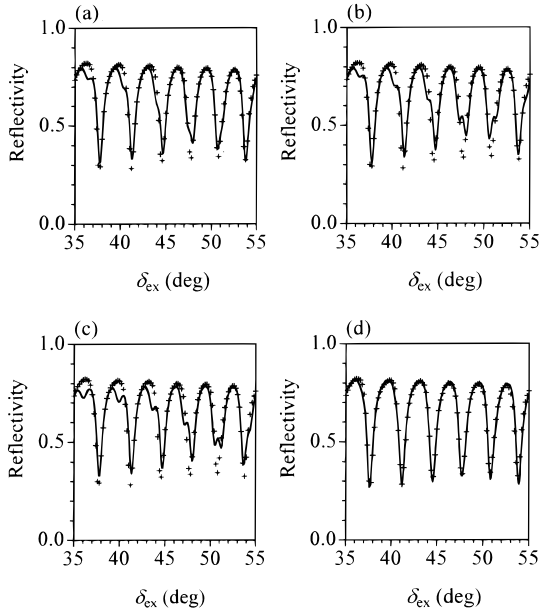

Figure 8. Effect of the rotational direction for the director of the PSiOFLC layer. The solid lines of each graph were calculated with the model illustrated in Figure 9. For details, see text.

waveguide mode patterns with *p*-light, fixed at $\beta = 90°$. The opposite movement of the resonance angle position against the case of *s*-light was seen. To analyze the switching process of the PSiOFLC, we tried to fit both TROWS data in the next section.

2.1. Data Analysis. The assumptions and definitions were made for the analysis of the transient waveguide mode patterns as follows:

The orientation of the director in the PSiOFLC layer is represented by a dielectric tensor in the dynamic states as well as both in the initial and final states. The geometry of the director is defined with three angles; the cone angle θ, the azimuthal angle ϕ, and the smectic layer tilt angle ψ. The geometry of the director is depicted in Figure 2b. We divided the PSiOFLC layer into two regions. This means that the transient layer structures of the PSiOFLC layer are expected to be deformed into a chevron geometry during the reorientation as elucidated for the low molecular mass FLC.[29] The total thickness of the PSiOFLC layer is kept constant throughout the reorientation process. The sum of the optic dielectric diagonals is also assumed to be constant. The numerical calculation of the angle-dependent reflectivity was done with the modified Berreman 4 × 4 matrix method, which is described in detail elsewhere.[35]

2.2. Rotational Direction during the Reorientation. Let us determine the direction of the rotational motion of the mesogenic groups around the smectic cone. Figure 8 shows the dependence of rotational direction on the transient waveguide mode pattern at $t = 42$ ms. The solid lines are theoretical curves calculated with the rotational models as depicted in Figure 9: (a) the mesogenic moieties rotate uniformly in the whole PSiOFLC layer with the bookshelf structure; (b) the mesogenic groups rotate simultaneously in the chevron structure; (c) the director rotates uniformly with the oblique bookshelf structure; (d) the mesogenic groups rotate toward the opposite direction between the top and bottom halves of the PSiOFLC layer. There are clear differences among parts a−d of Figure 8. Figure 8d

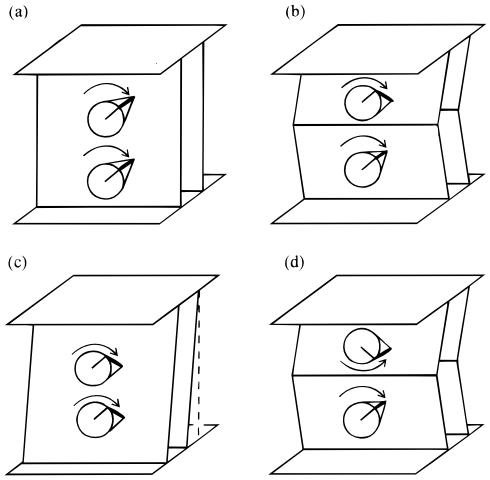

Figure 9. Model of the director rotation used in Figure 8. The layer structures are (a) a bookshelf structure, (b) a chevron structure, (c) an oblique bookshelf structure, and (d) a chevron structure. The smectic layer tilt angle was 5.7° for all graphs except for part a.

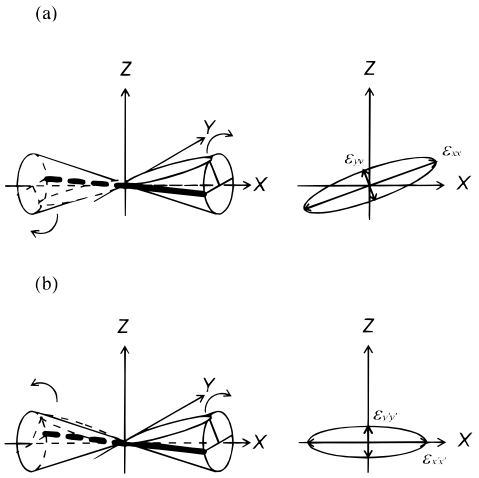

Figure 10. Optical rotational model for the PSiOFLC. The optic dielectric ellipsoid is tilted as shown in the right side of part a, while the dielectric ellipsoid on average reorients within the *XY* plane as shown in the right part of part b.

shows the best fitting among them, supporting the counterrotation of the directors in the chevron structure. This is the same as observed for 3M2CPOOB, probably attributed to the same surface effect of the substrate since both the 3M2CPOOB and the PSiOFLC layer were sandwiched between the same PI layers. Another plausible reason for the counter rotation is that the layer structure still has the memory of the previous chevron form at the beginning of the rotation. This means that the bookshelf structure under the electric field was not a perfect one, in particular at the interface with the substrate. Anyway the counterrotation model thus obtained will be applied to the following analyses.

2.3. Effect of the Molecular Motion. Comparison of each transient mode pattern, in particular from the viewpoint of the resonance angles in Figure 7, revealed that the waveguide mode pattern at 30 ms corresponds to that at the middle of the rotation, because the resonance angle starts going back toward the original position at this moment. In this section we discuss the mode of the motion of the mesogenic groups. Two models were considered as shown in Figure 10. One possible model is illustrated on the left side of Figure 10a. The polymer backbone lies between two smectic

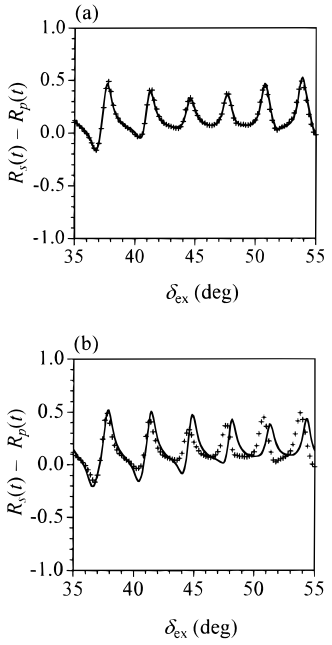

Figure 11. Fitting results for the subtraction $R_s(t) - R_p(t)$ obtained from the rotational model illustrated in Figure 10.

layer planes (the *YZ* plane). The director tip always points at the top of the cone which corresponds to the joint of branch from the polymer backbone. Two mesogenic side chains reorient around the cone synchronously with each other in the adjacent layers, fixing one end of the side chain to the polymer backbone. The other is the model that the mesogenic units rotate on the cone surface in opposite directions to each other as shown on the left side of Figure 10b. The rotational directions of the two directors are assumed to be opposite at the observation from the plus *X* axis. Each rotational model for the mesogenic units can be optically transfigured as follows. As shown on the right side of Figure 10a, an optical ellipsoid rotates around the smectic cone, keeping each component of diagonals, while in Figure 10b an optical ellipsoid on average moves on the *XY* plane.

To obtain a better fitting, we employed the difference of $R_s(t)$ and $R_p(t)$, i.e., $R_s(t) - R_p(t)$ at 30 ms. The time 30 ms corresponds to the midpoint of the reorientation as mentioned above. The fitting curve shown in Figure 11a is in good agreement with the experimental data. The theoretical curve in Figure 11b was calculated with the switching model shown in Figure 10b. This is not the case. The reason for the large difference between parts a and b of Figure 10 arises from the difference in the magnitudes of the dielectric diagonals. In Figure 10a, the components of the dielectric tensor are (ϵ_{xx}, ϵ_{yy}, ϵ_{zz}) = (2.579, 2.276, 2.276), while the average components in Figure 10(b) are ($\epsilon_{x'x'}$, $\epsilon_{y'y'}$, $\epsilon_{z'z'}$) = (2.543, 2.276, 2.312). These findings indicate that the mesogenic side chains rotate around the smectic cone in the same optical mode as the reorientation of the low molecular mass FLC. In other words the side chains reorient around the cone, keeping the balance at the center of gravity. This also indicates that the polymer main chain has little effect on the rotational mode of the mesogenic groups, although the switching rate becomes very slow due to the restriction from the polymer chain.

2.4. Effect of the Layer Structure. 2.4.1. Smectic Layer Tilt Angle. Figure 12 shows the effect of the smectic layer tilt angle on the reflectivity curves.

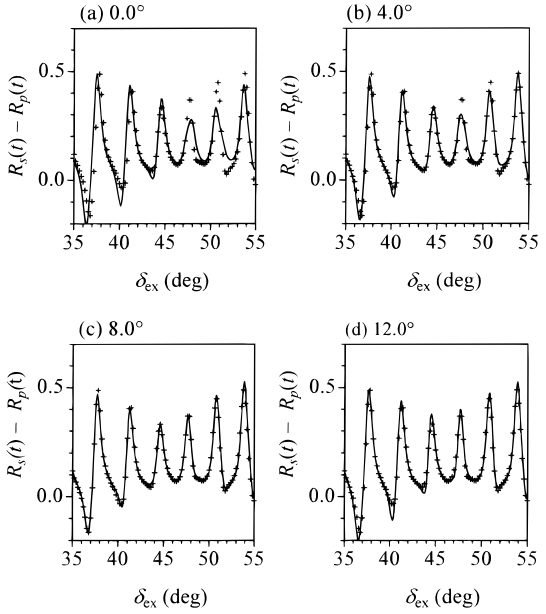

Figure 12. Effect of the smectic layer tilt angle ψ on $R_s(t) - R_p(t)$; the tilt angle gradually increases as follows: (a) 0.0°, (b) 4.0°, (c) 8.0°, and (d) 12.0°.

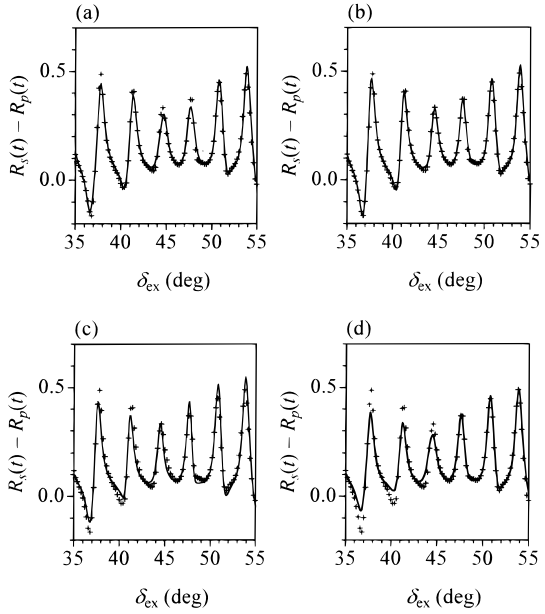

Figure 13. Effect of the chevron cusp position on $R_s(t) - R_p(t)$. The position of the chevron cusp changes as follows: (a) 33%, (b) 42%, (c) 50%, and (d) 59%.

To analyze the transient waveguide mode pattern we use the difference $R_s(t) - R_p(t)$ defined in section 2.3. In Figure 12a the theoretical curve was obtained using the model in which the mesogen moieties reorient around the cone constrained in the bookshelf structure. However, as described in section 2.2 and shown in Figures 8 and 9, the smectic layer is bent at the middle of the cell and takes a chevron structure during the reorientation. Such transient deformation (bookshelf−chevron−bookshelf) is called "layer buckling" during the reorientation. Parts b−d of Figure 12 show the tilt angle dependence of reflectivities at the midpoint of the reorientation. The values given in the caption of Figure 12 are for the layer tilt angles, by which the layer plane is tilted like a chevron. From the fitting, Figure 12c gave the best fit, signifying that the maximum smectic layer tilt angle was ca. 8.0° at the middle point of the reorientation.

2.4.2. Position of the Chevron Cusp. We discuss the effect of the cusp position in the chevron structure on the curve of $R_s(t) - R_p(t)$. In the case of the low molecular mass FLC (3M2CPOOB), the alignment of the molecules could be obtained by the two alignment layers which were rubbed in the same way.[29] The surface effect from each substrate on the FLC layer is therefore equivalent. In the case of the polymer FLC, however, the effect of the shearing procedure must be considered; only the bottom glass substrate was moved during the shearing procedure while the top substrate was fixed. This may cause an asymmetric influence to the FLCP from the top and the bottom surfaces, thus the position of the chevron cusp may not be at the center of the cell thickness. From the fitting shown in Figure 13, the cusp in the cell was estimated to lie at a distance of 42% thickness from the top surface. As Rieker et al. mentioned,[36] the asymmetric cusp in the S_{C^*} phase might be caused by the oblique bookshelf structure in the S_A phase. If this is the case, the tilting of the smectic layer would be observed in the S_A phase, but actually no layer tilting could be detected in the S_A phase.

2.5. Effect of the Optical Parameters. According to these reorientation models, the transient waveguide mode patterns were analyzed over the whole time range observed. Figure 14 shows the fitting results for both (a) *s*-light and (b) *p*-light. The theoretical curves are in good agreement with the experimental data obtained each time, although the simplified two-layer analysis was used. Next the dynamic properties of the PSiOFLC layer will be discussed in detail using the optical parameters obtained from the fitting.

2.5.1. Azimuthal Angle. Figure 15 shows the time dependence of the optical parameters obtained from the fitting: (a) azimuthal angle and (b) smectic layer tilt angle. As is obvious in Figure 15, the mesogenic side chains reorient around the cone in the millisecond range. Xue et al. reported an equation of the cone motion with respect to the azimuthal angle ϕ, which is given in eq 2, neglecting the small contribution from

$$\eta \frac{d\phi}{dt} = PE \sin \phi + \left(\frac{\Delta\epsilon}{4\pi}\right) E^2 \sin^2 \theta \sin \phi \cos \phi \quad (2)$$

the moment of inertia and the surface interactions,[37] with η being the rotational viscosity, $\Delta\epsilon$ the dielectric anisotropy at low frequency, E the electric field applied to the liquid crystal cell, and P the magnitude of the spontaneous polarization. The solid line in Figure 15a was obtained using eq 3, which is the numerical solution

$$t/\tau = \frac{1}{1-\alpha^2}\left\{\ln\frac{\tan(\phi/2)}{\tan(\phi_0/2)} + \alpha \ln\left[\frac{(1+\alpha\cos\phi)\sin\phi_0}{(1+\alpha\cos\phi_0)\sin\phi}\right]\right\} \quad (3)$$

for eq 2, with $\tau = \eta/PE$, $\phi_0 = \phi(t = 0)$, and $\alpha = \Delta\epsilon E(\sin^2\theta)/(4\pi P)$. When the proper parameters were chosen, a good agreement of both the azimuthal angles, calculated and observed, was found, although the contribution of the smectic layer tilt angle ψ is neglected in eq 2. In the case including the layer tilt angle, the two right terms in eq 2 are multiplied by $\cos\psi$ and $\cos^2\psi$. The maximum tilt angle was $\psi = 8.0°$, at which the values of $\cos\psi$ and $\cos^2\psi$ are 0.99 and 0.98, respec-

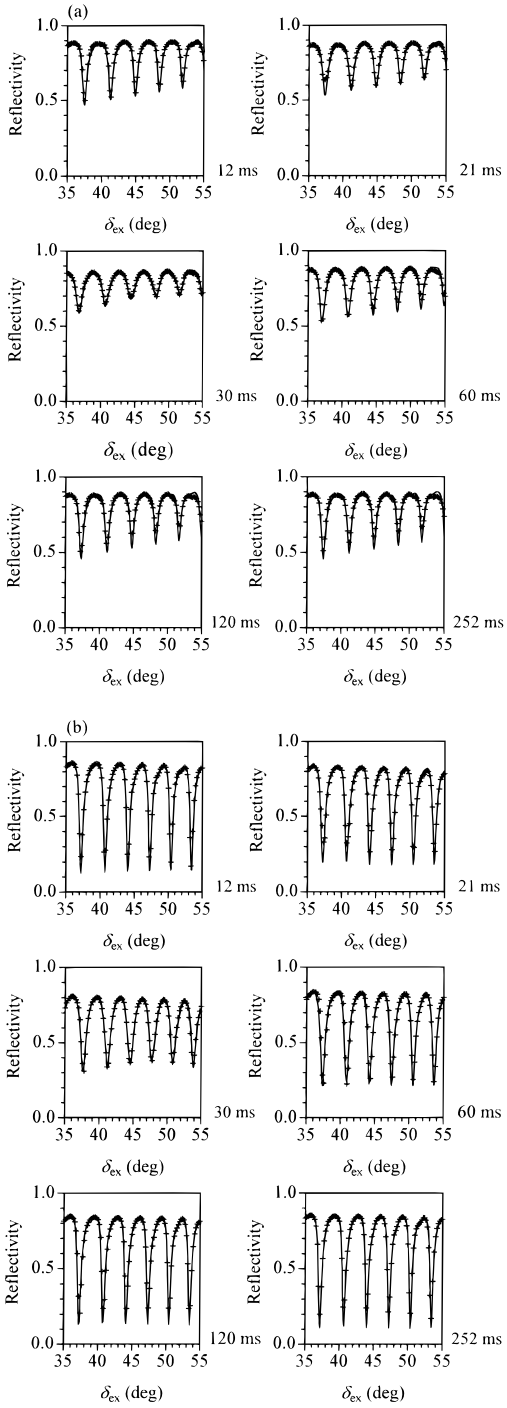

Figure 14. Fitting results of the transient waveguide mode patterns for (a) *s*-light and (b) *p*-light.

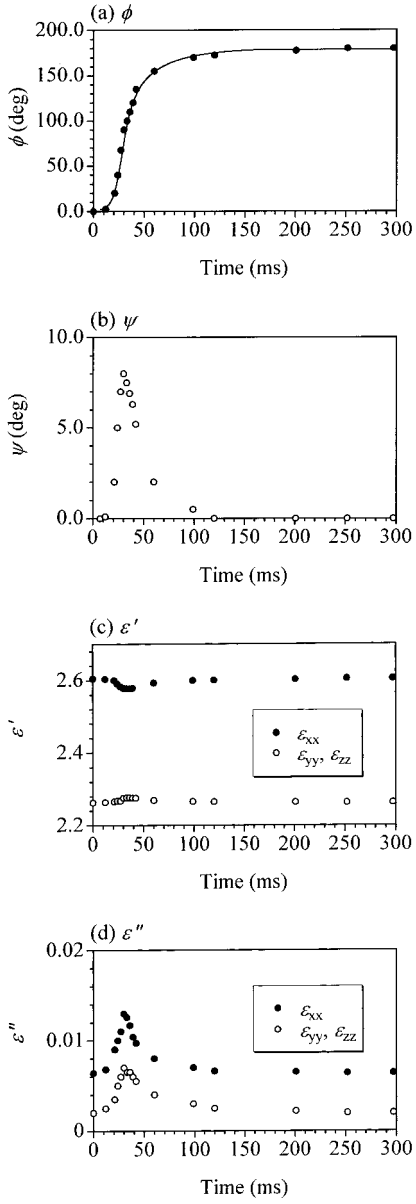

Figure 15. Time evolution of the optical parameters obtained from the fitting shown in Figure 14: (a) the azimuthal angle ϕ and (b) the smectic layer tilt angle ψ; (c) the real part and (d) the apparent imaginary part of the optic dielectric diagonals (ϵ_{xx}, ϵ_{yy}, ϵ_{zz}).

tively. This is the reason for the good agreement was seen between the experimental data and the theoretical curve of eq 3. From the fitting, not only were the parameters $\tau = 9.6$ ms, $\phi_0 = 0.5°$, and $\alpha = 0.75$ were obtained, but also the rotational viscosity was estimated as 5.08 Pa·s.[38] Comparing this value with the rotational viscosity of the low molecular mass FLC, the value for PSiOFLC is ca. 140 times larger than that for the low molecular mass FLC ($\eta = 0.037$ Pa·s for 3M2CPOOB). This indicates that the increase of the rotational viscosity is the most important factor responsible for the slower switching time. The increase of the rotational viscosity is due to the binding of mesogen groups to the polymer backbone. Kawasaki et al.[26] suggested that the polymer backbone moves synchronously with the mesogenic side chains during the reorientation. Furthermore, the spacer length between the mesogenic side chain and the polymer backbone influences the temperature range of the S_{C*} phase and the switching time. These findings suggest that the polymer backbone strongly affects the reorientation of the side chain FLCPs, retarding the cone motion of the side chain. This seems to be in disagreement with the finding obtained in section 2.3: the polymer backbone does not affect the mode of the motion. From these viewpoints the reorientation model will be discussed in section 3.

2.5.2. Smectic Layer Tilt Angle. The time evolution of the smectic layer tilt angle ψ is shown in Figure 15b. The PSiOFLC layer undergoes the layer buckling deformation as follows: The smectic layer is arranged from the initial bookshelf structure to the chevron like structure during the reorientation, and the smectic layer tilt angle reaches 8.0° at the maximum just halfway through the reorientation. This value is slightly smaller

than that evaluated by the X-ray diffraction measurement at static conditions.[39] Compared to the original chevron structure formed without electric field, the layer structure during the reorientation seems to be a nonequilibrium one, thus leading to the smaller layer tilt angle. The layer buckling during the reorientation could be attributed to the antiparallel dielectric interaction between the spontaneous polarization and the external electric field.[40] This also implies that the movement of the mesogenic side chains is similar to that of the low molecular mass FLC except for the point that the mesogenic moieties are strung together by the polymer backbone.

2.5.3. Real Part of the Optical Diagonals. Figure 15c shows the time course of the real part of the optic dielectric diagonals. The component parallel to the director of the mesogenic unit decreases from the initial value toward 30 ms, thereafter returning to the initial value. The components perpendicular to the director move in opposite directions, first an increase and then a decrease toward the initial value. This indicates that the mesogenic side chains reorient cooperatively but have some velocity distribution in the microscopic scale, although the deviation is rather small. In other words, the shrinkage of the optic dielectric ellipsoid reflects the orientational distribution around the mesogenic long axis of the PSiOFLC. This affects the optic dielectric tensor (ϵ_{xx}) to shrink along the director but increase in the plane perpendicular to the director (ϵ_{yy} and ϵ_{zz}). The maximum change for ϵ_{xx} was only 0.026. This value is similar to that for the 3M2CPOOB.[29] These values reflect the velocity distribution of mesogenic moieties. This also implies that the packing of the mesogenic moieties of the PSiOFLC is similar to that of the low molecular mass FLC.

2.5.4. Imaginary Part of the Optical Diagonals. Figure 15d shows the time course of the apparent imaginary part of the optic dielectric diagonals of the PSiOFLC. There is a somewhat anisotropic effect on the imaginary part. In this case the components parallel to the layer plane (ϵ''_{yy} and ϵ''_{zz}) were smaller than that perpendicular (ϵ''_{xx}) even at the initial and final states. The PSiOFLC itself has no absorption band at 632.8 nm. Therefore this anisotropy could be caused by light scattering resulting from the fluctuation of alignment of the side chains and/or inhomogeneity of the cell spacing induced by the unidirectional shearing. The larger contribution of ϵ''_{xx} implies the larger fluctuation of the smectic orientation in the direction of the layer normal.

During the reorientation, on the other hand, all components once increase and then decrease as seen in Figure 15d. In this case, the director undergoes the counter rotation between the top and the bottom halves of the PSiOFLC layer, which results in the nucleation of the disclination, i.e., discontinuity of the director, which may be one of the reasons for the light scattering during the reorientation. Another possible reason is a defect in the alignment. For the measurement of TROWS, the orientation of mesogenic groups was not perfect. A few defects such as the hairpin and thunder shapes still remain in the cell. These possibly become the defective points where the transient disclination easily appears during reorientation,[41] resulting in the increase of the imaginary part.

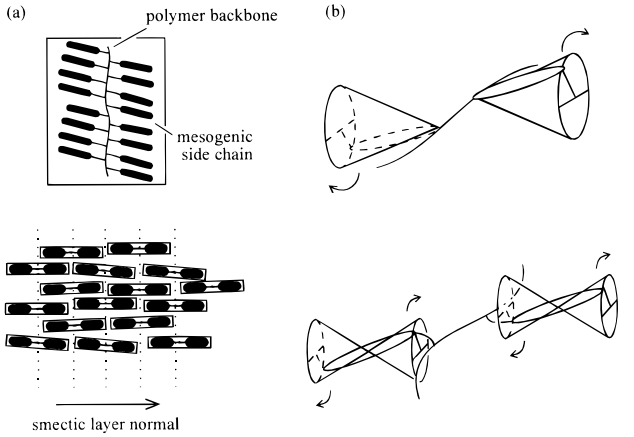

Figure 16. (a) Top: Conformation of a ferroelectric liquid crystalline polymer illustrated from the top view. Bottom Side view of the packing of the polymer block.[43] (b) Top: mesogenic side chain rotating around the top of cone. Bottom: Mesogenic side chain rotating around the center of double cones.

In conclusion, the motion of the mesogenic side chains is the same as that of the low molecular mass FLC, the difference being only the switching time range.

3. Reorientation Model. Before discussing the reorientational model, let us consider the molecular area to estimate the molecular packing. The cone angle θ correlates the molecular area of two aromatic cores as $\cos\theta = 2\rho_{ar}/S$ where ρ_{ar} is the molecular area of the aromatic cores ($\rho_{ar} \cong 22-24$ Å^2)[42] and S the molecular area occupied in the smectic plane by the two molecules. The observed tilt angle was 20.0°, resulting in $S = 48$ Å^2. Clearly this suggests a monolayer arrangement of tilted aromatic cores. The molecular area of a dimethylsiloxane monomer ρ_{si} has been evaluated as ca. 19 Å^2.[43] Thus, the molecular area of the backbone is smaller than that of mesogenic units.

From the result of the molecular area, the mesogenic groups interdigitate with each other from both sides of the smectic layer. The schematic illustration in Figure 16a shows the top and side views of the layer structure.[44−51] In PSiOFLC, the thickness of the smectic layer corresponds to the side chain length, obtained by the X-ray measurement.[52]

Under this layer structure, the side chains can reorient around the cone as shown in the upper part of Figure 16b. The results in Figures 10 and 11 indicate that one of the side chains rotates clockwise (right), while the other rotates counterclockwise (left) with respect to the observer sitting on the polymer main chain. In this model the polymer backbone does not move during the reorientation. This seems to be inconsistent with the results by time-resolved FT-IR showing that the polymer backbone moves synchronously with the mesogenic groups.[26]

It is also possible to consider the model shown in the lower part of Figure 16b. The position of the center of motion and the scale of the molecular motion is different in the top and bottom models in Figure 16b. The mesogenic units in the bottom can reorient around the cones in half scale of those in the top; the volume necessary for the motion is four times larger in the top model than in the bottom model. In the bottom case, the side chains reorient around the cone in the same manner as the 3M2CPOOB molecules, although they must tow the polymer backbone during the reorientation; most but not all of the whole side chain including

the aromatic cores and several methylene spacers take part in the reorientation. As Kawasaki et al.[14] reported previously, the methylene spacer promotes the decoupling between the main chains and the mesogenic groups, resulting in the decrease of the switching time. The methylene spacer may act to release the side chain from the polymer backbone, although it still draws the polymer backbone. Thus the side chains reorient around the cone, keeping its center of gravity in the side chain, although the motion must be coupled with the main chain to some extent.

Conclusion

The static structures and the switching dynamics of the side chain ferroelectric liquid crystalline polymer (PSiOFLC) were investigated by time-resolved optical waveguide spectroscopy. The optical characterization in each phase was done carefully. We obtained a good alignment of the mesogenic side chains by shearing the cell at the isotropic−S_A phase transition. Since the contribution of the main chain to the optical anisotropy was negligibly small, the PSiOFLC layer could be treated as a uniaxial optical ellipsoid which aligned parallel to the substrate plane in the S_A phase. In the S_{C^*} phase, the PSiOFLC layer was arranged from chevron to bookshelf structure when a high electric field was applied. The optic ellipsoid in the S_{C^*} phase was also considered as a uniaxial one. The molecular motion of PSiOFLC was similar to that of the low molecular mass FLC from the optical point of view, except for the switching time; that is, the molecular motion of the side chains, in particular the mode of motion, is not influenced by the polymer backbone. The slowness of the switching time is ascribed to a "polymer effect": the polymer backbone lying in the smectic layer plane acts as a "hook" to restrict the motion of side chains due to the binding of the mesogenic moieties to the polymer backbone, which is responsible for the increase of the rotational viscosity. The stabilization of the liquid crystalline phase is also attributed to the "polymer effect", resulting in the enhancement of the alignment stability.

Acknowledgment. This work was supported by a Grant-in-aid for Scientific Research (No. 07651105) by the Ministry of Education, Science, Sports, and Culture of Japan. M.M. would like to thank the Japan Society for the Promotion of Science for a Research Fellowship.

References and Notes

(1) Shibaev, V. P.; Kozlovsky, M. V.; Beresnev, L. A.; Blinov, L. M.; Platé, N. A. *Polym. Bull.* **1984,** *12*, 299.
(2) Decobert, G.; Soyer, F.; Dubois, J. C. *Polym. Bull.* **1985**, *14*, 179.
(3) Guglielminetti, J. M.; Decobert, G.; Dubois, J. C. *Polym. Bull.* **1986**, *16*, 411.
(4) Hahn, B.; Percec, V. *Macromolecules* **1987**, *20*, 2961.
(5) Uchida, S.; Morita, K.; Miyoshi, K.; Hashimoto, K.; Kawasaki, K.; *Mol. Cryst. Liq. Cryst.* **1988**, *155*, 93.
(6) Kitazume, T.; Ohnogi, T.; Ito, K. *J. Am. Chem. Soc.* **1990**, *112*, 6608.
(7) Gray, G. W.; Hill, J. S.; Lacey, D. *Makromol. Chem.* **1990**, *191*, 2227.
(8) Bata, L.; Csorba, K. F.; Szabon, J.; Kozlovsky, M. V.; Holly, S. *Ferroelectrics* **1991**, *122*, 149.
(9) Endo, H.; Hachiya, S.; Sekiya, T.; Kawasaki, K. *Liq. Cryst.* **1992**, *12*, 147.
(10) Poths, H.; Andersson, G.; Skarp, K.; Zentel, R. *Adv. Mater.* **1992**, *4*, 792.
(11) Hsu, C. S.; Lin, J. H.; Chou, L. R.; Hsiue, G. H. *Macromolecules* **1992**, *25*, 7126.
(12) Hsu, C. S.; Shih, L. J.; Hsiue, G. H. *Macromolecules* **1993**, *26*, 3161.
(13) Fadel, H.; Percec, V.; Zheng, Q.; Advincula, R. C.; Duran, R. S. *Macromolecules* **1993**, *26*, 1650.
(14) Kawasaki, K.; Moriwaki, F.; Hachiya, S.; Endo, H.; Sekiya, T.; Hashimoto, K. *Ferroelectrics* **1993**. *148*, 245.
(15) Verrall, M.; Beattie, D.; Coates, D.; Sage, I.; Lymer, K. *Ferroelectrics* **1996**, *181*, 327.
(16) Skarp, K.; Andersson, G.; Lagerwall, S. T.; Kapitza, H.; Poths, H.; Zentel, R. *Ferroelectrics* **1991**, *122*, 127.
(17) Bettig, W.; Naciri, J.; Shashidhar, R.; Duran, R. S. *Macromolecules* **1991**, *24*, 6539.
(18) Nazemi, A.; Williams, G.; Attard, G. S.; Karasz, F. E. *Polym. Adv. Technol.* **1992**, 3, 157.
(19) Giesselmann, F.; Zugenmaier, P.; Scherowsky, G.; Kühnpast, K.; Springer, J. *Makromol. Chem. Rapid Commun.* **1992**, *13*, 489.
(20) Zentel, R.; Poths, H.; Kremer, F.; Schönfeld, A.; Jungbauer, D.; Twieg, R.; Willson, C. G.; Yoon, D. *Polym. Adv. Technol.* **1992**, *3*, 211.
(21) Sekiya, T.; Yuasa, K.; Uchida, S.; Hachiya, S.; Hashimoto, K.; Kawasaki, K. *Liq. Cryst.* **1993**, *14*, 1255.
(22) Xue, Q. B.; Chen, X.; Yang, K. Z. *Macromol. Chem. Phys.* **1995**, *196*, 3243.
(23) Takahashi, K. I.; Ishibashi, S.; Yamamoto, F. *Ferroelectrics* **1996**, *181*, 277.
(24) Uto, S.; Moritake, H.; Myojin, K.; Ozaki, M.; Yoshino, K.; Skarp, K.; Helgee, B. *Ferroelectrics* **1996**, *181*, 297.
(25) Svensson, M.; Helgee, B.; Skarp, K.; Andersson, G.; Hermann, D. *Ferroelectrics* **1996**, *181*, 319.
(26) Kawasaki, K.; Kidera, H.; Sekiya, T.; Hachiya, S. *Ferroelectrics* **1993**, *148*, 233.
(27) Shilov, S. V.; Okretic, S.; Siesler, H. W.; Zentel, R.; Öge, T. *Macromol. Rapid Commun.* **1995**, *16*, 125.
(28) Shilov, S. V.; Skupin, H.; Kremer, F.; Gebhard, E.; Zentel, R. *Liq. Cryst.* **1997**, *22*, 203.
(29) Mitsuishi, M.; Ito, S.; Yamamoto, M.; Fischer, T.; Knoll, W. *Mol. Cryst. Liq. Cryst.* in press.
(30) Manthis, A.; Haziioannou, G.; Skoulios, A. *Polym. Eng. Sci.* **1977**, *17*, 570.
(31) Mitsuishi, M.; Ito, S.; Yamamoto, M.; Fischer, T.; Knoll, W. *J. Appl. Phys.* **1997**, *81*, 1125.
(32) Sprokel, G. J. *Mol. Cryst. Liq. Cryst.* **1981**, *69*, 39.
(33) Davidson, P.; Levelut, A. M. *Liq. Cryst.* **1992**, *11*, 469 and references therein.
(34) Brandrup, J.; Immergut, E. H. *Polymer Handbook*, 2nd ed.; Wiley: New York, 1975; p IV-382.
(35) Ito, S.; Kremer, F.; Fischer, T.; Knoll, W.; *Mol. Cryst. Liq. Cryst.* **1995**, *264*, 99.
(36) Rieker, T. P.; Clark, N. A.; Smith, G. S.; Parmar, D. S.; Sirota, E. B.; Safinya, C. R. *Phys. Rev. Lett.* **1987**, *59*, 2658.
(37) Xue, J. Z.; Handschy, M. A.; Clark, N. A. *Ferroelectrics* **1987**, *73*, 305.
(38) The magnitudes of the spontaneous polarization for PSiOFLC and 3M2CPOOB are assumed to be 10 nC/m^2 and 100 nC/cm^2, respectively.
(39) Yuasa, K.; Uchida, S.; Sekiya, T.; Hashimoto, K.; Kawasaki, K. *Polym. Adv. Technol.* **1992**, *3*, 205.
(40) Hartmann, W. J. A. M.; Vertogen, G.; Gerritsma, C. J.; Sprang, H. A. v.; Verhulst, A. G. H. *Europhys. Lett.* **1989**, *10*, 657.
(41) Fukuda, A.; Takezoe, H. *Structures and Properties of Ferroelectric Liquid Crystals*; Corona: Tokyo, 1990; p 379.
(42) Guillon, D.; Skoulios, A.; Benattar, J. J. *J. Phys.* (*Paris*) **1986**, *47*, 133.
(43) Lenk, T. J.; Lee, D. H. T.; Koberstein, J. T. *Langmuir* **1994**, *10*, 1857.
(44) Zugenmaier, P.; Mügge, J. *Makromol. Chem. Rapid Commun.* **1984**, *5*, 11.
(45) Ebbutt, J.; Richardson, R. M.; Taylor, L.; Blackwood, K. M.; Sage, I. C.; Beattie, D. R.; Verrall, M. *Ferroelectrics* **1996**, *181*, 261.
(46) Noirez, L.; Cotton, J. P.; Hardouin, F.; Keller, P.; Moussa, F.; Pépy, G.; Strazielle, C. *Macromolecules* **1988**, *21*, 2889.
(47) Hardouin, F.; Noirez, L.; Keller, P.; Lambert, M.; Moussa, F.; Pepy, G.; Richard, H. *Mol. Cryst. Liq. Cryst.* **1988**, *155*, 389.
(48) Davidson, P.; Noirez, L.; Cotton, J. P.; Keller, P. *Liq. Cryst.* **1991**, *10*, 111.
(49) Mensinger, H.; Biswas, A. *Polym. Adv. Technol.* **1992**, *3*, 257.
(50) Noirez, L. *Mol. Cryst. Liq. Cryst.* **1995**, *261*, 525.
(51) Noirez, L.; Lapp, A. *Phys. Rev. E* **1996**, *53*, 6115.
(52) Endo, H. Personal communication.

MA971433Y